Microwave Spectra of Noble Gas–Pyridine Dimers: Argon–Pyridine and Krypton–Pyridine

T. D. Klots, T. Emilsson, R. S. Ruoff, and H. S. Gutowsky*

Noyes Chemical Laboratory, University of Illinois, Urbana, Illinois 61801 *(Received: April 1, 1988; In Final Form: July 25, 1988)*

Rotational spectra were observed for dimers of argon and krypton with pyridine (Pyr) by using a Flygare–Balle Fourier transform microwave spectrometer. The dimers are prolate near symmetric tops. Rotational constants were determined for several isotopic species of each. For Ar–Pyr, we found A, B, and C to be 2990.327 (7), 1207.862 (1), and 1199.335 (2) MHz, and D_J, D_{JK}, and D_K to be 3.58 (5), 19.6 (1), and −23.5 (15) kHz. The corresponding values for ^{84}Kr–Pyr are 2986.703 (1), 806.9294 (1), and 803.0235 (2) MHz and 1.370 (5), 8.74 (7), and −9.4 (2) kHz. Nuclear quadrupole coupling constants were determined from the hyperfine structure of the rotational transitions for dimers with one or more of the quadrupole nuclei ^{14}N, D, or ^{83}Kr. Analysis of the data shows that the Ar/Kr is above the pyridine ring on a plane of symmetry containing the pyridine center of mass (cm) and the nitrogen. The pyridine cm to rare gas vector R is 3.545 Å for the dimer with Ar and 3.648 Å for Kr. R is rotated from the vertical by ~3.5° toward the nitrogen (−3.5°). The pyridine axis perpendicular to its plane oscillates about the equilibrium position with an average displacement of ~7°. A simple pseudodiatomic model for the interaction potential gives the stretching force constant to be 0.0270 and 0.0351 mdyn/Å for the Ar–Pyr and Kr–Pyr dimers, with well depths of 232 and 322 cm^{-1}. In ^{83}Kr–Pyr the electric field gradient (EFG) at the Kr has near-axial symmetry with χ_z = −4.722 MHz in the ab plane and the z axis rotated away from the nitrogen by 26.7° from the vertical (+26.7°). Calculation of the electric field gradient with an electric, distributed multipole expansion model gives results agreeing semiquantitatively with experiment.

I. Introduction

Rotational spectra, accurate structures, and other properties have been determined for many weakly bonded dimers, especially those in which hydrogen bonding is important. Considerable progress has been made in the theoretical interpretation of these results. An attractive approach is the electrostatic model based on the interactions among the permanent electric moments of the monomers and their mutual polarization, including dispersion effects.[1,2] The repulsion on close approach of the monomers is simulated by hard spheres at the atomic centers. The geometry of many of the simpler dimers has been predicted successfully in this manner.[3] The simplest case, the linear structure so often found for AB–HX dimers, is favored by a pure, electric dipole–(induced) dipole interaction. However, when larger monomers and higher electric moments are involved, the distribution of the multipoles on the monomers also needs to be considered, and the analysis becomes more complex.

Virtually all of the dimers characterized so far by rotational spectroscopy contain monomers with one to four atoms. Only a handful have an aromatic ring. Therefore, the Ar/Kr–pyridine dimers appealed to us as likely subjects for extending our knowledge in this direction. Pyridine is a weak base in water and a good hydrogen-bond acceptor. Moreover, it has a large dipole moment along the C_{2v} axis. Accordingly, a pyridine–HF dimer in the gas phase would be expected to have a linear, or nearly linear, >N:···H–F hydrogen bond. However, chemical experience so far is a less reliable guide in predicting the structure of a complex between pyridine (Pyr) and a noble-gas atom such as Ar or Kr.

Several experimental studies of dimers between a noble-gas atom and an aromatic molecule have found the atom above the molecular plane. Laser-induced fluorescence electronic spectra of Ar–benzene[4] and of He/Ar with s-tetrazine[5,6] showed that in these dimers the rare-gas atom is over the center of the ring. Of course, benzene and s-tetrazine do not have an electric dipole moment, so axial dimers are not unexpected. The Ar–furan dimer has been studied by Fourier transform (FT) microwave spectroscopy and found to have the argon above the furan plane.[7] However, furan has a relatively small dipole moment (0.66 D), and the larger moment of pyridine (2.22 D) might lead to a planar, "linear" dimer for it. So a study of the Ar/Kr dimers with pyridine seemed in order.

The microwave spectra of several isotopic species of Ar/Kr–Pyr dimers were observed by using the pulsed nozzle, FT microwave method. In them, we find that the Ar or Kr is indeed above the ring on a vertical plane of symmetry, as in Ar–furan, in spite of the much larger dipole moment of pyridine. Results for Ar–[4-D]Pyr show that the Ar/Kr is displaced slightly toward the ring nitrogen. The stretching force constant and binding strength of the interaction are estimated with a simple centrifugal distortion analysis. Also the nuclear quadrupole coupling induced in ^{83}Kr by dimer formation has been measured in both the [^{14}N]- and [^{15}N]Pyr complexes. The experimental results are compared with electric field gradients calculated with several types of electric multipole distributions for the pyridine.

II. Experimental Section

Rotational spectra were observed by using the pulsed nozzle FT microwave technique on the Flygare Mark II spectrometer. Details of the spectrometer operation have been described previously.[8] Pyridine is a liquid at room temperature with a vapor pressure of ~20 mmHg, so a stream of carrier gas was bubbled through the liquid, becoming saturated. The dimers with Ar could be made directly by diluting the argon and pyridine stream with more Ar, all at a total pressure of 12 psi. The flowing gas mixture was pulsed with a solenoid valve (General Valve) on a 1-mm-diameter nozzle, and the overflow gas was pumped away. Spectra were optimized at pyridine concentrations of around 0.4%. The free induction decay (FID) could be made stronger (×4) by using neon "first run" (70% Ne, 30% He) as the carrier gas, with about 5% Ar or Kr, and a backing pressure of 25 psi. This procedure was used for all of the Kr–Pyr dimers.

The ^{40}Ar–[^{15}N]Pyr dimer was observed at natural abundance while for ^{83}Kr–[^{15}N]Pyr, 99% labeled [^{15}N]pyridine was used

(1) Buckingham, A. D.; Stone, A. J. *Int. Rev. Phys. Chem.* **1986**, *5*, 107.
(2) Dykstra, C. E. *J. Phys. Chem.* **1987**, *91*, 6216.
(3) Buckingham, A. D.; Fowler, P. W. *Can. J. Chem.* **1985**, *63*, 2018.
(4) Fung, K. H.; Selsle, H. L.; Schlag, E. W. *Z. Naturforsch.* **1981**, *36A*, 1338.
(5) Smalley, R. E.; Wharton, L.; Levy, D. H.; Chandler, D. W. *J. Chem. Phys.* **1978**, *68*, 2487.
(6) Haynam, C. A.; Brumbaugh, D. V.; Levy, D. H. *J. Chem. Phys.* **1984**, *80*, 2256.
(7) Kukolich, S. G.; Shea, J. A. *J. Chem. Phys.* **1982**, *77*, 5242. Kukolich, S. G. *J. Am. Chem. Soc.* **1983**, *105*, 2207.
(8) Campbell, E. J.; Read, W. G.; Shea, J. A. *Chem. Phys. Lett.* **1983**, *94*, 69.

0022-3654/89/2093-1255$01.50/0

TABLE I: Observed and Fitted Unperturbed Line Centers for the Rotational Transitions of Ar–Pyr, Ar–[4-D]Pyr, and ^{84}Kr–Pyr[a]

Ar–pyridine[b]				Ar–[4-D]pyridine[c]		^{84}Kr–pyridine[c]	
trans	obsd, MHz	I	II	trans	obsd, MHz	trans	obsd, MHz
$0_{00} \rightarrow 1_{11}$	4189.6361	−1	5	$0_{00} \rightarrow 1_{11}$	4065.5168	$0_{00} \rightarrow 1_{11}$	3789.7139
$1_{01} \rightarrow 2_{02}$	4814.2430	0	−5	$1_{01} \rightarrow 2_{12}$	6419.6054	$1_{01} \rightarrow 2_{12}$	5395.6876
$1_{11} \rightarrow 2_{12}$	4805.6595	−2	−14	$1_{11} \rightarrow 2_{12}$	4733.6315	$1_{10} \rightarrow 2_{21}$	9763.0393
$1_{10} \rightarrow 2_{11}$	4822.7280	−1	0	$1_{01} \rightarrow 2_{02}$	4758.7190	$1_{11} \rightarrow 2_{20}$	9766.9500
$1_{01} \rightarrow 2_{12}$	6588.1195	0	−3	$1_{10} \rightarrow 2_{11}$	4784.2238	$2_{12} \rightarrow 3_{13}$	4823.7974
$1_{10} \rightarrow 2_{21}$	10170.1330	0	10	$2_{11} \rightarrow 2_{20}$	5058.2377	$2_{02} \rightarrow 3_{03}$	4829.6895
$1_{11} \rightarrow 2_{20}$	10178.6994	1	19	$2_{12} \rightarrow 2_{21}$	5133.8473	$2_{11} \rightarrow 3_{12}$	4835.5137
$3_{12} \rightarrow 3_{21}$	5334.4203	−1	−3			$2_{02} \rightarrow 3_{13}$	6999.6261
$2_{12} \rightarrow 3_{03}$	5447.2048	0	−3			$3_{13} \rightarrow 3_{22}$	6556.7289
$2_{02} \rightarrow 3_{13}$	8982.1437	1	−6			$3_{03} \rightarrow 4_{14}$	8601.5045
$4_{14} \rightarrow 4_{23}$	5317.2331	2	−9			$4_{04} \rightarrow 5_{15}$	10201.3018
$3_{03} \rightarrow 4_{14}$	11371.6684	1	1				
$5_{14} \rightarrow 5_{23}$	5295.9973	1	−16				
$4_{22} \rightarrow 5_{15}$	6610.0331	0	1				
$6_{15} \rightarrow 6_{24}$	5270.8889	1	−15				
$7_{17} \rightarrow 7_{26}$	5477.0170	0	−3				
$7_{16} \rightarrow 7_{25}$	5242.1098	2	−3				
$8_{17} \rightarrow 8_{26}$	5209.8942	−2	20				

[a] For details of the hfs and fitting it to determine the line centers listed here and the quadrupole coupling constants in Table IV, see: Klots, T. D. Ph.D. Thesis, 1988, University of Illinois. [b] Fit I uses the parameters A, B, C, τ_1, τ_2, τ_{aaaa}, τ_{bbbb}, and τ_{cccc}; fit II uses A, B, C, D_J, D_{JK}, and D_K. The residue given is obsd − calcd, in kHz. [c] The rms deviation with fit II is 0.6 kHz.

(Cambridge Isotope Laboratories). The [4-D]pyridine was synthesized locally in a two-step preparation. Isonicotinic acid (0.4 mol) was exchanged isotopically with an excess of D_2O (4 mol) at the boiling point. The labeled isonicotinic acid was then heated in the presence of CuO, with trapping and purification of the pyridine product. The prepared sample was determined to be 55% [4-D]pyridine by NMR and mass spectroscopy. The balance of the product was mostly pyridine. We thank Tom Govani for assistance in the preparation.

Transitions were observed in the 3–12-GHz range by averaging the FIDs at 8 Hz on an LSI-11. The time-domain spectra were then Fourier transformed into the power spectra. Hyperfine structure (hfs) caused by the nuclear quadrupole moments of the ^{14}N, D, and ^{83}Kr nuclei was readily resolved for the isotopic species containing these nuclei (Figure 1). The standard deviation of frequencies for hyperfine components or unsplit transitions is generally 1 kHz except for Ar–[4-D]pyridine, where it is 2 kHz.

III. Results and Analysis

A. Search, Hyperfine Structure, and Rotational Constants. Pyridine is an oblate near symmetric top with its a axis coincident with the C_2 axis through the nitrogen. Binding of an Ar (or Kr) above the ring then gives a prolate near symmetric rotor as found for the Ar–furan dimer.[7] In this event the a axis of the heterocycle becomes the b axis of the dimer (Figure 2), and the dipole moment lies primarily along it. Our search for the Ar–Pyr dimer therefore began in C band for b type rotational transitions using the Ar to furan center-of-mass (cm) distance (3.54 Å) as a guide. The $0_{00} \rightarrow 1_{11}$ transition with its set of hyperfine structure (hfs) was soon found, followed by several other b–dipole transitions. These were used to locate the three $J = 1 \rightarrow 2$ a–dipole transitions near 4810 MHz. Though expected to be weak, they were in fact observed with decent signal to noise. On the basis of the optimum pulse length and power for the a and b type transitions, we estimate the a component of the dipole moment to be about 1/20 the b component.[9] The dipole moment of pyridine is ~2.2 D, so this indicates an a component of 0.1 D. Once the Ar–Pyr dimer was characterized, similar procedures were used for the krypton analogues.

The Hamiltonian used to fit the hfs for each of the dimers is the sum of rotational and nuclear quadrupole parts:

$$H = H_R + H_Q(1) + H_Q(2) \quad (1)$$

H_R is the rotational Hamiltonian and H_Q the quadrupole Hamiltonian; the latter includes terms for each of the quadrupolar nuclei ^{14}N, D, and ^{83}Kr in the dimer in question. Matrix elements of H_Q were evaluated in the coupled basis set $F = J + I_N$ for the Ar/^{84}Kr–[^{14}N]Pyr dimers, where $I_N = 1$. For the Ar–[4-D]Pyr and ^{83}Kr–Pyr dimers the basis set was $F = J + I$, where $I = I_N + I_{D/Kr}$ and $I(^{83}Kr) = 9/2$. The hf components were fitted by using an asymmetric top program with χ_{aa} and $(\chi_{bb} - \chi_{cc})/\sqrt{6}$ as adjustable parameters. The inertial axes of the dimers are rotated from the principal axes of the quadrupole interactions so the off-diagonal elements of χ_{gg} ($g = a,b,c$) are nonzero. However, their magnitudes are too small to contribute significantly to the second-order quadrupole energy.[10] Initial, approximate sets of rotational constants were used to fit the hfs and determine the line centers.

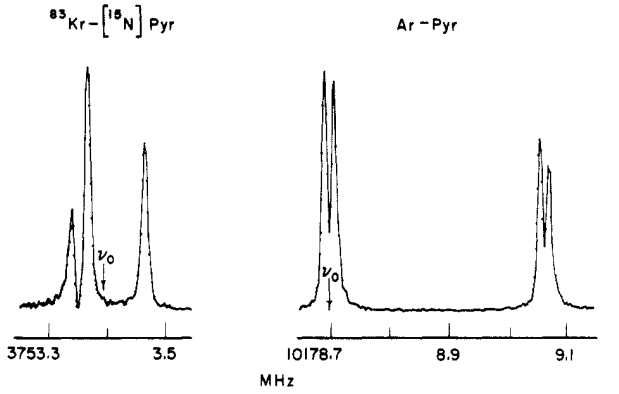

Figure 1. Hyperfine structure for the $0_{00} \rightarrow 1_{11}$ transition of the ^{83}Kr–[^{15}N]Pyr dimer (left) centered at 3753.390 MHz, and two of the three components for the $1_{11} \rightarrow 2_{20}$ transition of Ar–Pyr (right) at 10178.699 MHz. The Doppler doubling was suppressed for the spectrum at the left but not at the right. The calibration is 1.6276 kHz/point. For the spectrum at the left 1652 FIDs were accumulated, and at the right, 359.

The hfs observed for Ar–Pyr, Ar–[4-D]Pyr, and ^{84}Kr–Pyr and its analysis are uneventful, and the details are not included here. The unperturbed line centers determined by the fitting are listed in Table I, which includes a reference to the hfs. The most complex hfs measured is that for the ^{83}Kr–Pyr dimer. Only two of its transitions were observed and fitted (Table II), enough to determine the diagonal elements of the ^{83}Kr quadrupole coupling tensor. A few other transitions were observed and assigned for

(9) Campbell, E. J.; Buxton, L. W.; Balle, T. J.; Flygare, W. H. *J. Chem. Phys.* **1981**, *74*, 813. Campbell, E. J.; Buxton, L. W.; Keenan, M. R.; Balle, T. J.; Flygare, W. H. *J. Chem. Phys.* **1981**, *74*, 829.

(10) Gordy, W.; Cook, R. L. *Microwave Molecular Spectra*; Wiley: New York, 1984; Chapter IX.

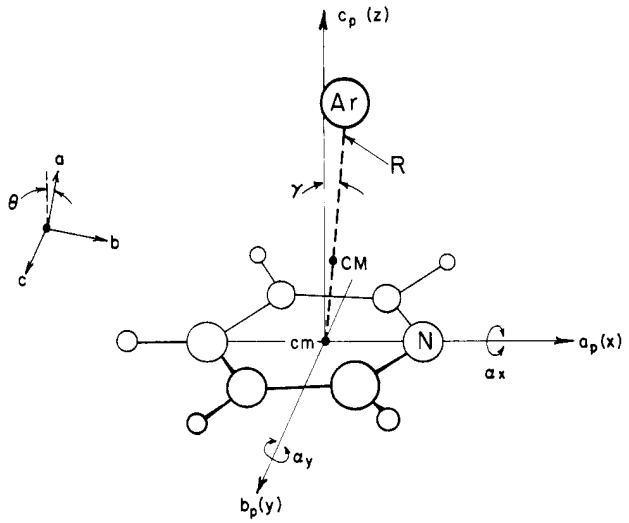

Figure 2. Schematic structure and coordinate system for the argon–pyridine dimer. Distances are to scale except γ and θ are increased 2-fold. The axes a_p, b_p, and c_p (x,y,z) are the principal axes of pyridine monomer, and a,b,c are those for the dimer. R is the line joining the argon and the center of mass of the pyridine, and CM is the center of mass of the dimer.

TABLE II: Observed and Fitted Hyperfine Components for the Rotational Transitions of ^{83}Kr–Pyridine

transition $J_{K_pK_o} \rightarrow J'_{K_pK_o}$	component[a] $I,F \rightarrow I',F'$	obsd, MHz	obsd − calcd, kHz
$0_{00} \rightarrow 1_{11}$	7/2,7/2 → 7/2,9/2		
	11/2,11/2 → 7/2,9/2	3792.4987	0.2
	11/2,11/2 → 11/2,11/2		
	9/2,9/2 → 9/2,9/2	3792.5418	−2.0
	7/2,7/2 → 9/2,7/2		
	9/2,9/2 → 9/2,7/2	3792.5565	2.7
	7/2,7/2 → 7/2,5/2	3793.9281	−2.7
	11/2,11/2 → 11/2,13/2	3793.9529	0.9
	9/2,9/2 → 9/2,9/2		
	11/2,11/2 → 9/2,11/2	3794.0098	0.0
	9/2,9/2 → 9/2,11/2		
	7/2,7/2 → 11/2,9/2		
	11/2,11/2 → 11/2,9/2	3796.1467	1.0
	9/2,9/2 → 11/2,9/2		
$1_{01} \rightarrow 2_{12}$	7/2,9/2 → 11/2,11/2	5406.1900	−0.5
	7/2,9/2 → 7/2,9/2	5406.2052	5.3
	9/2,11/2 → 11/2,11/2	5406.4042	0.2
	9/2,7/2 → 7/2,7/2	5406.4762	1.8
	9/2,11/2 → 11/2,13/2	5406.5470	1.6
	9/2,7/2 → 9/2,5/2	5406.6618	2.2
	11/2,9/2 → 9/2,11/2	5407.9241	1.0
	11/2,9/2 → 9/2,11/2	5407.9761	−6.2
	11/2,13/2 → 11/2,15/2	5408.0143	−3.7
	7/2,7/2 → 9/2,7/2	5408.1211	1.9
	11/2,11/2 → 9/2,13/2	5408.1764	0.3
	7/2,7/2 → 7/2,5/2	5408.2964	2.2

[a] $I = I_N + I_{Kr}$.

^{82}Kr, ^{86}Kr, and ^{15}N isotopic species of the dimer (Table III). They include the $0_{00} \rightarrow 1_{11}$ transition of ^{83}Kr–[^{15}N]Pyr. From its observed hfs (Figure 1), χ_{bb} was found for ^{83}Kr. The hyperfine interaction constants determined for the isotopic species in Tables I–III are summarized in Table IV.

The most extensive set of line centers (18) is for the Ar–Pyr dimer. Two procedures were employed to find its rotational constants. In fit I the Kirchoff program, CDANAL, for a distortable asymmetric rotor was used to determine A, B, C, and the five independent fourth-order centrifugal distortion constants.[11] Fit II treated the complex as a distortable near symmetric top, with the three symmetric top distortion constants, D_J, D_{JK}, and D_K. The residues of the two fits are compared in Table I. It is apparent that fit I with CDANAL is significantly better. It fits the observed frequencies with a root-mean-square (rms) deviation of 1.2 kHz, while fit II has 9.8 kHz. Fit I needs a minimum of 10 transitions, so it was used only for Ar–Pyr. The rotational constants from the two fits are given in Table V. The differences are minor.

Seven line centers were measured for Ar–[4-D]Pyr and eleven for ^{84}Kr–Pyr (Table I). The results of fitting them with the near

(11) Kirchoff, W. H. *J. Mol. Spectrosc.* **1972**, *41*, 333.

TABLE III: Other Transitions Observed and Assigned[a]

dimer	transition $J_{K_pK_o} \rightarrow J'_{K_pK_o}$	component $F \rightarrow F'$	obsd, MHz
^{40}Ar–[^{15}N]Pyr	$0_{00} \rightarrow 1_{11}$	no hfs	4146.935
^{82}Kr–Pyr	$0_{00} \rightarrow 1_{11}$	1 → 1	3796.6603
^{82}Kr–[^{15}N]Pyr	$0_{00} \rightarrow 1_{11}$	no hfs	3757.5007
^{83}Kr–Pyr	$0_{00} \rightarrow 1_{11}$	line center[b]	3793.7363 (15)
	$1_{01} \rightarrow 2_{12}$	line center[b]	5407.7210 (11)
^{83}Kr–[^{15}N]Pyr	$0_{00} \rightarrow 1_{11}$	9/2 → 9/2	3753.3392
		9/2 → 11/2	3753.3629
		9/2 → 7/2	3753.4612
^{84}Kr–[^{15}N]Pyr	$0_{00} \rightarrow 1_{11}$	no hfs	3749.3821
^{86}Kr–Pyr	$0_{00} \rightarrow 1_{11}$	1 → 1	3780.7086
		1 → 2	3782.1549
	$1_{01} \rightarrow 2_{12}$	1 → 2	5371.1443
		2 → 2	5372.1550
		2 → 3	5372.6201
		0 → 1	5374.3978

[a] Observed at natural abundance: ^{15}N, 0.37%; ^{82}Kr, 12%; ^{83}Kr, 12%; ^{84}Kr, 57%; ^{86}Kr, 17%. [b] Obtained from fit of hfs in Table II.

TABLE IV: ^{14}N, D, and ^{83}Kr Nuclear Quadrupole Coupling Constants (MHz)[a] in the Inertial Axis System of the Dimers[b]

dimer	nucleus	χ_{aa}	χ_{bb}	χ_{cc}
Ar–Pyr	^{14}N	3.3648 (25)	−4.8053 (20)	1.4406 (25)
Ar–[4-D]Pyr	^{14}N	3.342 (4)	−4.784 (4)	1.442 (4)
	D	−0.108 (4)	0.186 (4)	−0.078 (4)
^{84}Kr–Pyr	^{14}N	3.3743 (12)	−4.8164 (11)	1.4421 (14)
^{83}Kr–Pyr[b]	^{14}N	3.374[c]	−4.816[c]	1.442[c]
	^{83}Kr	−2.875 (10)	0.509 (11)	2.366 (11)
^{83}Kr–[^{15}N]Pyr	^{83}Kr	−2.908 (13)[d]	0.542 (2)	2.366 (11)[e]

[a] The numbers in parentheses are 1 standard deviation of the fit. [b] For ^{83}Kr, the components in the principal axis system of the field gradient, χ_x, χ_y, and χ_z, are 2.356, 2.366, and −4.722 MHz, respectively. [c] These values from ^{84}Kr–Pyr were assumed and held fixed in fitting the hfs for ^{83}Kr in this dimer. [d] Determined from the condition $\sum_g \chi_{gg} = 0$. [e] Value taken from the results for ^{83}Kr–[^{14}N]Pyr.

TABLE V: Rotational Constants Determined for the Ar–Pyridine Dimer by Fitting Line Centers to Asymmetric Rotor and Symmetric Top Models

CDANAL asym rotor[a]		sym top model	
const	value, MHz	const	value, MHz
A	2990.3460 (10)	A	2990.3266 (70)
B	1207.8901 (4)	B	1207.8621 (14)
C	1199.3552 (3)	C	1199.3346 (15)
τ_1	−0.1202 (1)	D_J	0.00358 (5)
τ_2	−0.03136 (4)	D_{JK}	0.0196 (1)
τ_{aaaa}	−0.0044 (8)	D_K	−0.0235 (15)
τ_{bbbb}	−0.0141 (2)		
τ_{cccc}	−0.0135 (1)		
rms dev of fit, kHz	1.2		9.8

[a] Reference 11.

TABLE VI: Rotational Constants Determined for Ar–[4-D]Pyr and ^{84}Kr–Pyr[a]

const	Ar–[4-D]Pyr	^{84}Kr–Pyr
A, MHz	2888.417 (2)	2986.7034 (1)
B, MHz	1202.4264 (15)	806.9294 (1)
C, MHz	1177.1294 (17)	803.0235 (2)
D_J, kHz	3.4 (2)	1.370 (5)
D_{JK}, kHz	18.5 (4)	8.74 (7)
D_K, kHz	−21.1 (6)	−9.4 (2)

[a] Constants determined from fit II of unperturbed line centers.

TABLE VII: Approximate Values of A, B, and C Determined for ^{84}Kr–[^{15}N]Pyr and Two ^{83}Kr–Pyr Dimers

const	^{84}Kr–[^{15}N]Pyr	^{83}Kr–[^{14}N]Pyr	^{83}Kr–[^{15}N]Pyr
A, MHz	2953.11 (1)	2986.705 (10)	2953.11 (1)
B, MHz	802.84 (1)	810.98 (1)	806.92 (1)
C, MHz	796.656 (7)	807.06 (1)	800.67 (1)

TABLE VIII: Comparison of Planar Moments (amu Å^2) for the Dimers with the Corresponding Values for Pyridine[a]

moment	Ar–Pyr	Ar–[4-D]Pyr	^{84}Kr–Pyr
P_a	335.3931	337.3319	543.2173
P_b	85.9898	92.0000	86.1280
P_c	83.0148	82.9676	83.0817
P_a'	87.0800	93.2604	87.0800
P_b'	83.7018	83.7042	83.7018
$P_c - P_b'$	−0.6870	−0.7366	−0.6201
$P_b - P_a'$	−1.0902	−1.2604	−0.9520

[a] Moments for the dimers were calculated with the rotational constants from fit II, and the primed moments for pyridine and [4-D]-pyridine with the constants in Table IX. A conversion factor of 50.537 907 × 10^4 amu Å^2/s was used for $I \times B$.

symmetric top method (fit II) are listed in Table VI. The residues are small for both dimers, the rms deviation of 0.6 kHz constrasting with the 9.8 kHz found for fit II of Ar–Pyr. The difference reflects the use of more transitions for the latter (18 versus 7 and 11), extending to higher J's. If the 11 $J \leq 4$ transitions are fitted for Ar–Pyr, the rms deviation drops to 0.7 kHz, the same as for ^{84}Kr–Pyr. For consistency in the structural analysis we use the rotational constants from the near symmetric top treatment (fit II) for all three species. Approximate values of A, B, and C for three other isotopic species of Kr–Pyr are listed in Table VII. They were estimated from the transitions in Table III and the structural parameters determined for ^{84}Kr–Pyr.

B. Molecular Symmetry and Structure. The asymmetry parameter κ is −0.9905 for Ar–Pyr and −0.9964 for ^{84}Kr–Pyr, both very close to the prolate symmetric top limit of −1. This requires that the noble-gas atom be near to c_p, the c axis of pyridine, approximately over the center of the pyridine ring (Figure 2). Symmetry favors locating the Ar/Kr atom in the plane perpendicular to the pyridine ring and containing a_p, the pyridine C_2 axis. We show this to be the case by comparing the planar moments P_c of the dimers with the corresponding planar moment P_b' of pyridine itself. P_c is defined as[12]

$$P_c = \tfrac{1}{2}(I_a + I_b - I_c) = \sum_i m_i c_i^2 \qquad (2)$$

from which P_a and P_b are obtained by cyclic permutation. P_c describes the extent to which the masses m_i are distributed away from the ab plane, i.e., with $c_i \neq 0$. Changes in m_i for which $c_i = 0$ do not affect P_c. Note that the ab plane of the dimer corresponds to the a_pc_p plane of the pyridine.

Table VIII lists the planar moments for the three dimers whose rotational constants have been determined most accurately: Ar–Pyr, Ar–[4-D]Pyr, and ^{84}Kr–Pyr. It is seen that P_c is virtually the same for all three dimers, ~83 amu Å^2. The 4-D substitution in Ar–Pyr decreases P_c by 0.0472 amu Å^2, while replacement of ^{40}Ar by ^{84}Kr increases it by 0.1141. These small changes in P_c are attributed to vibrational differences, and it is concluded that all four atoms are in the ab plane of the dimers, making it a symmetry plane.

As a consequence, for a rigid dimer in which the structure of the pyridine is unchanged from the free molecule, P_c is determined by the inertial properties of pyridine or [4-D]pyridine alone.[13] Inspection of Figure 2 shows that P_c should equal P_b', the planar moment P_b of free pyridine, the spectroscopic properties of which are summarized in Table IX.[13] Comparison of the planar moments in Table VIII shows that while $P_c \cong P_b'$, the value of P_c is consistently about 0.68 amu Å^2 less in the three dimers than P_b' is in the free pyridines. An effect of this sign and magnitude is consistent with vibrations of the pyridine in which it oscillates about an in-plane axis. Rotation of the pyridine about the b_p axis does not affect P_c, but rotation by α_x about a_p (Figure 2) changes eq 2 for P_c to

$$P_c = \sum_i m_i (c_i^\circ)^2 \cos^2 \alpha_x = P_b' \cos^2 \alpha_x \qquad (3)$$

Moreover, the oscillation must be symmetrical with respect to the ab plane, otherwise the latter is not a plane of symmetry. Therefore, the ratios P_c/P_b' observed for the three dimers correspond to "average" angular displacements $\alpha_x \equiv \arccos \langle \cos^2 \alpha_x \rangle^{1/2}$.[14] The planar moments in Table VIII give these to be 5.20, 5.38, and 4.94°.

Rotation of the pyridine by a_y about the b_p axis has a similar effect upon P_b of the dimer. However, although the c axis of the dimer coincides with the b_p axis, the ab axes are rotated by several degrees from a_pc_p. This modifies the contributions of pyridine and the rare-gas atom to P_b and necessitates a different approach to determine a_y. Nonetheless, P_b for the dimers is only about 1.1 amu Å^2 less than P_a' of pyridine (Table VIII), indicating that the angular displacements are small.

The moments of inertia determined for each dimer can give us three structural parameters. Having established that the ab plane of the dimers is a plane of symmetry, we take as unknowns the pyridine cm to rare-gas atom distance R and the angle γ between R and the equilibrium position of the pyridine c_p (vertical) axis as shown in Figure 2. The third unknown is the "average" angular displacement α of the c_p axis from its equilibrium position, where α is related to the torsional oscillations of pyridine about its a_p and b_p axes by the equation

$$\tan^2 \alpha = \tan^2 \alpha_x + \tan^2 \alpha_y \qquad (4)$$

We now express the inertial tensor for the dimers in terms of these unknowns, using an x,y,z coordinate system which corresponds to a_p,b_p,c_p for the equilibrium position of the pyridine. This gives[7,12]

$$I_{yy} = I_b(\mathrm{Pyr})\langle 1 + \tfrac{1}{2} \sin^2 \alpha \rangle + \mu R^2 \qquad (5a)$$

$$I_{xx} = I_a(\mathrm{Pyr})\langle 1 + \tfrac{1}{2} \sin^2 \alpha \rangle + \mu R^2 \cos^2 \gamma \qquad (5b)$$

$$I_{zz} = I_c(\mathrm{Pyr})\langle 1 - \tfrac{1}{2} \sin^2 \alpha \rangle + \mu R^2 \sin^2 \gamma \qquad (5c)$$

$$I_{xz} = -\mu R^2 \sin \gamma \cos \gamma \qquad (5d)$$

where μ is the reduced mass of the dimer treated as a pseudodiatomic species. The other elements of the matrix are zero.

The xz 2 × 2 block in eq 5 is readily diagonalized, giving[10]

$$I^{\pm} = \tfrac{1}{2}(I_{zz} + I_{xx}) \pm \tfrac{1}{2}(I_{zz} - I_{xx})(1 + \tan^2 2\theta)^{1/2} \qquad (6)$$

Here I^+ is I_a(dimer), I^- is I_b(dimer), and $\tan 2\theta = 2I_{xz}/(I_{zz} - I_{xx})$,

TABLE IX: Spectroscopic Properties of Pyridine Monomer and Its 4-D and ^{15}N Derivatives

property[a]	Pyr[b]	[4-D]Pyr[b]		[^{15}N]Pyr[c]	
A	6039.2516 (6)	6038.9967 (10)		6039.45 (8)	
B	5804.9116 (6)	5420.0697 (9)		5680.37 (6)	
C	2959.2117 (6)	2855.8194 (8)		2926.54 (2)	
$\chi_a(^{14}\mathrm{N})$	−4.908 (3)	−4.907 (3)[d]			
χ_b	1.434 (3)	1.442 (5)			
χ_c	3.474 (3)	3.465 (5)			
Q_{aa}[e]	−3.5	χ_a(D)[d]	0.196 (4)	μ_a	2.215
Q_{bb}	9.7	χ_b	−0.090 (8)		
Q_{cc}	−6.2	χ_c	−0.106 (8)		

[a] Units are megahertz except for μ, which is in debye, and Q_{gg}, which is in debye angstrom. Coordinates a,b,c are here the inertial axes of the pyridine. [b] Reference 13a. [c] Reference 13b. [d] Reference 13c. [e] Reference 25.

(12) Shea, J. A.; Flygare, W. H. *J. Chem. Phys.* **1982**, *76*, 4857.
(13) (a) Mata, F.; Quintant, M. J.; Sørensen, G. O. *J. Mol. Struct.* **1977**, *42*, 1. (b) Sørensen, G. O.; Hansen, L.; Rostrup-Andersen, N. *J. Mol. Struct.* **1974**, *20*, 119. (c) Heineking, N.; Driezler, H.; Schwarz, R. *Z. Naturforsch.* **1986**, *41A*, 1210.
(14) Ruoff, R. S.; Emilsson, T.; Chuang, C.; Klots, T. D.; Gutowsky, H. S. *Chem. Phys. Lett.* **1987**, *138*, 553.

TABLE X: Structural Parameters Obtained by Inertial Analysis for the Ar–Pyr, Ar–[4-D]Pyr, ^{84}Kr–Pyr, and Ar–Furan Dimers[a]

dimer	R, Å	γ, deg	θ, deg	α, deg	α_x, deg	α_y, deg
Ar–Pyr	3.5453	−3.511	−4.706	7.225	5.198	5.046
Ar–[4-D]Pyr	3.5470	−3.971	−5.443	7.221	5.383	4.841
^{84}Kr–Pyr	3.6480	−3.401	−4.034	6.854	4.938	4.777
Ar–furan[b]	3.5410	−5.463	−6.509	12.188	8.679	8.689

[a] See Figure 2 and eq 4 for definition of symbols. [b] Calculated by using the rotational constants in ref 7.

where θ is the angle by which the principal axis system of the dimer is rotated about its c axis from the x,y,z pyridine system. Also, I_c (dimer) is I_{yy}. With these relationships, an iterative grid search was used to determine the values of R, γ, and α that best fit the three experimental moments of inertia for each dimer. The results of the fit are listed in Table X for the three dimers. For Ar–Pyr, magnitudes of 3.5453 Å, 3.511°, 4.706°, and 7.225° were found for R, γ, θ, and α, respectively. (Our γ corresponds to the θ employed for the Ar–furan dimer.[7])

Isotopic substitution must be used to determine whether the rare-gas atoms is rotated toward or away from the nitrogen. 4-D substitution moves the pyridine cm away from the nitrogen along the a_p axis. Therefore, if γ is negative (R rotated toward the nitrogen), the 4-D substitution moves the pyridine cm away from the rare-gas atom, increasing R, and vice versa. In Table X, the R for Ar–[4-D]Pyr is appreciably longer than for Ar–Pyr, 3.5470 versus 3.5453 Å, showing that R is rotated toward the nitrogen. Similar reasoning accounts for the larger magnitudes of γ and θ in Ar–[4-D]Pyr than in Ar–Pyr.

Equation 5 assumes that the torsional vibrations of the pyridine are isotropic in the dimers even though one of the axes involved is a symmetry axis and the other is not. An indication of the actual anisotropy can be gained by using eq 4 to calculate α_y with the α's from the inertial analysis by eq 5 and the α_x's from the planar moments by eq 3. These results for α, α_x, and α_y are summarized in Table X, where it may be seen that α_y is consistently smaller by ~5% than α_x, the difference being largest for the dimer with [4-D]Pyr.

The magnitude found for γ in ^{84}Kr–Pyr is very close to that of Ar–Pyr, 3.401° versus 3.511°. Therefore it seems likely that R is rotated toward the nitrogen for the Kr species as well as for the Ar. Experimental evidence in support of this is mentioned in section III.D.

C. Vibrational Analysis. Upon attachment of an argon or krypton atom to pyridine, three translational degrees of freedom are lost. They are replaced by three low-frequency, van der Waals vibrational modes—the two nearly degenerate torsional vibrations of the pyridine about its a_p and b_p axes and a pseudodiatomic stretch between the Ar/Kr atom and the pyridine cm. These three modes cause most of the vibrational effects in the dimer, including not only the inertial effects just analyzed but also a reduction in the ^{14}N quadrupole coupling and the centrifugal distortion D_J.

For weak dimers, the electric field gradients suffer little or no change from those in the monomers,[15] and we assume this in the present case. However, the tensor(s) of each monomer (Table IX) are projected upon the inertial axes of the dimer, and the projection is vibrationally averaged over the zero-point motions of the dimer.[16] In pyridine the ^{14}N quadrupole coupling has components of −4.908, 1.434, and 3.474 MHz, respectively, in the a_p, b_p, and c_p (x,y,z) inertial axis system of the monomer. The values for [4-D]pyridine differ only slightly. In the Ar–Pyr dimer, the ^{14}N coupling has components of 3.3648, −4.8053, and 1.4406 MHz, now in the principal axes a, b, and c of the dimer, with very similar results for Ar–[4-D]Pyr and ^{84}Kr–Pyr (Table IV). Thus, the main effect upon $\chi(^{14}N)$ of forming the dimer is to permute the axes: $a_p,b_p,c_p \rightarrow b,c,a$; also χ_{aa}(dimer) and χ_{bb}(dimer) become about 0.10 MHz smaller, while χ_{cc}(dimer) is virtually unchanged. This confirms the orientation of the axes given in Figure 2 and indicates that the a,b axes of the dimer are rotated slightly about the $c(b_p)$ axis from the c_p,a_p axes of pyridine.

TABLE XI: Pseudodiatomic Potential Constants for Dimers of a Noble-Gas Atom with an Aromatic Molecule

dimer	k_s, mdyn/Å	ν_s, cm^{-1}	R_e, Å	ϵ, cm^{-1}
Ar–Pyr	0.0270	41.5	3.509	232
Kr–Pyr	0.0351	38.2	3.621	322
Ar–furan[a]	0.0269	42.5	3.503	236

[a] Reference 7.

Actually, the reduction in χ_{aa} and χ_{bb} for the dimer from the corresponding components in the monomer is a combination of a static axis rotation and time-dependent vibrations. The information available is insufficient for an accurate deconvolution of their effects. However, an approximate analysis can be made by using standard methods[10] to relate χ_{gg} for the dimer to χ_i of the monomer, the transformation enabling one to solve for $\theta + \alpha_y$ and for α_x. For Ar–Pyr, they are found to be 6.36 and 3.26°, respectively. These values are about 2° smaller than those from the inertial analysis (Table X). The differences are small enough to reflect the approximations of the model. Similar results are obtained from an analysis of the ^{14}N and D coupling constants for Ar–[4-D]Pyr and ^{84}Kr–Pyr.

The centrifugal distortion may be used to estimate the pseudodiatomic stretching force constant. The calculation can be made in terms of either the τ's for an asymmetric top or D_J for a symmetric top. In the case of the Ar–furan dimer, the two approaches gave the same result,[7] so we use the simpler D_J relation.[17] With it, we find a stretching force constant, k_s, of 0.0270 mdyn/Å for the Ar–Pyr dimer and 0.0351 mdyn/Å for ^{84}Kr–Pyr, which correspond[18] to stretching frequencies of 41.5 and 38.2 cm^{-1}, respectively. Finally, by assuming a Lennard-Jones 6-12 potential we estimate ϵ, the dimer well depth,[7,19] to be 232 and 322 cm^{-1} for the pyridine dimers with Ar and Kr. The results for the noble gas–pyridine/furan dimers are summarized in Table XI.

D. ^{83}Kr Nuclear Quadrupole Coupling. The nonzero quadrupole coupling of ^{83}Kr in the ^{83}Kr–Pyr dimers indicates that the electron distribution of the Kr is polarized by its interactions with pyridine. The diagonal elements χ_{aa}, χ_{bb}, and χ_{cc} of the quadrupole coupling tensor were determined for both the ^{83}Kr–[^{14}N]Pyr and ^{83}Kr–[^{15}N]Pyr dimers[20] by fitting the rotational hfs. This gives the coupling constants in the principal inertial axes of the dimer (Table IV). However, to better visualize the interaction, we transform it to the principal axes (x,y,z) of the electric field gradient (EFG) at the Kr nucleus, finding[10]

$$\chi_{aa} = \chi_x \sin^2 \beta + \chi_z \cos^2 \beta \quad (7a)$$

$$\chi_{bb} = \chi_x \cos^2 \beta + \chi_z \sin^2 \beta \quad (7b)$$

$$\chi_{cc} = \chi_y \quad (7c)$$

Here, $\beta \equiv \theta_{za}$ is the angle between the z axis of the field gradient and the a inertial axis of the ^{83}Kr–[^{14}N]Pyr dimer.

The ab plane is a plane of symmetry, so χ_y is the same as χ_{cc}. This leaves three unknowns (χ_x, χ_y, and β) and only two observed quantities (χ_{aa} and χ_{bb}). However, by using the coupling constants for both ^{83}Kr–[^{14}N]Pyr and ^{83}Kr–[^{15}N]Pyr, we can solve for the unknowns. The substitution of ^{15}N for ^{14}N rotates the inertial axes about the c axis by a small amount δ, giving another pair of equations like eq 7a and 7b but with somewhat different values of χ_{aa}', χ_{bb}', and $\beta' = \beta + \delta$. Because of their symmetry the four

(15) Keenan, M. R.; Buxton, L. W.; Campbell, E. J.; Legon, A. C.; Flygare, W. H. *J. Chem. Phys.* **1981**, *74*, 2133. Soper, P. D.; Legon, A. C.; Read, W. G.; Flygare, W. H. *J. Chem. Phys.* **1982**, *76*, 292.

(16) Klots, T. D.; Chuang, C.; Ruoff, R. S.; Emilsson, T.; Gutowsky, H. S. *J. Chem. Phys.* **1987**, *86*, 5315.

(17) Read, W. G.; Campbell, E. J.; Henderson, G. *J. Chem. Phys.* **1983**, *78*, 3501.

(18) Buxton, L. W.; Campbell, E. J.; Keenan, M. R.; Balle, T. J.; Flygare, W. H. *Chem. Phys.* **1981**, *54*, 173.

(19) Balle, T. J.; Campbell, E. J.; Keenan, M. R.; Flygare, W. H. *J. Chem. Phys.* **1980**, 72, 922.

(20) For the ^{83}Kr–[^{15}N]Pyr dimer only χ_{bb} was measured. However, χ_{cc} should be the same as in the [^{14}N]Pyr dimer, enabling χ_{aa} to be calculated.

equations are not independent. The angular dependence (β and β') can be separated from χ_x and χ_z by taking the ratio ρ of ($\chi_{aa}' - \chi_{bb}'$) to ($\chi_{aa} - \chi_{bb}$), whereby

$$(1 - 2\sin^2\beta') = \rho(1 - 2\sin^2\beta) \quad (8)$$

Equation 8 can be solved iteratively for β if the angle δ between the inertial axes of the two dimers is known.

In ^{84}Kr–[^{14}N]Pyr the inertial analysis showed the dimer's a axis to be rotated −4.034° from the pyridine c_p axis (θ in Table X). A similar calculation with the approximate rotational constants of the ^{84}Kr–[^{15}N]Pyr dimer (Table VII) gives a rotational angle of −3.729° for it. Further analysis showed that the difference of 0.305° should be the same for the ^{83}Kr–Pyr dimers to at least four significant digits. Therefore we take δ to be −0.305°, noting that the a' axis for the dimer with ^{15}N is at a *larger* angle from the nitrogen than is the a axis of the ^{14}N species.

With δ = −0.305°, eq 8 gives a value of +30.720° for β and +30.415° for β'. In eq 7a and 7b this result for β leads to values of −4.722 and 2.356 MHz for χ_z and χ_x, respectively. Furthermore, in order that $\beta > \beta'$, the z axis of the electric field gradient must be rotated away from the nitrogen, i.e., counterclockwise in Figure 1, making an angle of +26.7° with respect to the pyridine c_p axis. This angle has an estimated uncertainty of ±8°. The values for χ_y (χ_{cc}) is 2.366 MHz, nearly identical with the 2.356 MHz found for χ_x, so the EFG is symmetric about the z axis.

In the linear, rare-gas (Rg) dimers Rg–HX and Rg–HCN, the quadrupole coupling constant χ_a observed for ^{83}Kr and ^{131}Xe has been a useful guide to the interactions between the rare-gas atom and the HX and HCN molecules.[21] An electric multipole expansion was used with the multipole located at the cm of the dipolar species to calculate the electric field and its gradient (eq_a°/h) along the a axis at the position of the Rg. This long-range polarization model, using the first few moments of HX and HCN, gives good agreement with experiment, indicating there is little or no charge transfer between the Rg and HX or HCN species in the dimers. We have tried a similar approach to the ^{83}Kr–Pyr dimer, with somewhat mixed results.

The elements χ_{gg} of the ^{83}Kr quadrupole coupling tensor are given by

$$\chi_{gg} = -eQq_{gg}^\circ(1 - \gamma_\infty)/h \quad (9)$$

where Q, the nuclear electric quadrupole moment of ^{83}Kr, is taken to be 0.27 b,[22] and q_{gg}° is the gg element of the EFG at the site of the Kr, produced by the pyridine molecule. The Sternheimer shielding parameter γ_∞ translates the externally applied field gradient q° to that at the Kr nucleus; for it we use Campbell's value of −79 ± 15.[21] The EFG tensor was calculated from the potential $\vec{V}$ generated at the Kr site by the pyridine, expressed in polymatrix form.[23,24]

$$\vec{V} = -T\cdot\vec{M} \quad (10)$$

T is a first-degree polytensor, and $\vec{M}$ contains the electrical moments of pyridine. Experimental values are available for only the molecular dipole[13] and quadrupole[25] moments of pyridine (Table IX). Placing them at the pyridine cm, we calculated the elements of q_{gg}° at the Kr in the inertial axis system of the pyridine. We then diagonalized the tensor to obtain its principal axis system, with elements χ_i as defined for the experimental values.

The results, combined with eq 9, give quadrupole coupling constants χ_x, χ_y, and χ_z of 7.2, 12.4, and −19.6 MHz, with the z axis rotated away from the nitrogen, making an angle of +8.6° with respect to the pyridine c_p axis (Figure 1). The calculated values are 4 times too large, but the direction of the principal axis and the near axial symmetry are in more reasonable agreement with experiment. The calculation does not include vibrational averaging, but "tilt" of the pyridine z axis would reduce χ_z by at most a few percent. Inclusion of the pyridine octupole moment would have a larger effect, reducing χ_z by perhaps 20%,[26] but still not nearly enough.

TABLE XII: Comparison of the Experimental ^{83}Kr Quadrupole Coupling Tensor (MHz) with Calculations for Several Multipole Models

model[a]	χ_x	χ_y[b]	χ_z	θ, deg[c]
I	7.2	12.4	−19.6	+8.6
II	1.84	4.36	−6.20	−1.5
III	0.85	3.31	−4.16	+0.8
IV	1.06	3.88	−4.94	+9.7
V	0.98	3.44	−4.42	+5.0
exptl	2.356	2.366	−4.722	+26.7

[a] Model I is with the dipole and quadrupole at the pyridine cm. Models II–V are with distributed multipoles; see text for details. [b] This corresponds to χ_{cc} in Table VI. [c] θ is here defined as the angle between the principal axis (z) of the EFG at the krypton and the c_p axis of pyridine.

The failure of the simple, multipole expansion model in this case is probably because pyridine is much larger than HX and HCN and is relatively much closer to the Kr. So the convergence of a series expansion for the electric field gradient is much slower. One way of circumventing this problem is to distribute the charge and multipoles over the molecule, constraining the distribution to reproduce selected molecular properties. For pyridine at least four such distributed multipole models have been generated, primarily because of theoretical interest in the energetics and long-range forces of azabenzene crystals. Each model attempts to fit the experimental molecular dipole and quadrupole moments at some level. The models include the following types: II, point charges at C, H, and N atoms and the lone pair;[27] III, same as II but with different point charges;[27] IV, dipoles along the C–H bonds and the N to lone-pair vector;[28] V, point charges, dipoles, and quadrupoles at the C and N atoms.[29] Evaluation of the EFG from eq 10 remains straightforward for these models. The results for χ_i are summarized in Table XII, including those calculated with the dipole and quadrupole located at the pyridine cm (I) and the experimental values. All four distributed multipole models give coupling constants significantly lower than the cm multipole model, in semiquantitative agreement with experiment.[30] Type V is perhaps the best, with χ_x, χ_y, and χ_z being 0.98, 3.44, and −4.42 MHz and a rotation angle θ of +5°.

IV. Discussion

Our findings are consistent with and extend the earlier work on dimers of a noble-gas atom with an aromatic molecule. The Ar/Kr–Pyr dimers have the noble-gas atom centrally located above the plane of the aromatic ring as in the argon–furan dimer[7] as well as in the more symmetric Ar–benzene[4] and He/Ar–s-tetrazine[5,6] dimers. In fact the Ar to pyridine cm distance R (3.545 Å) is virtually the same as that (3.544 Å) reported for Ar–furan.[7] The corresponding distance for Ar–s-tetrazine is significantly shorter (3.44 Å), indicative probably of the four nitrogens and their smaller radius. That for Ar–benzene is also short (3.4 Å), but its estimated error is large (0.2 Å).

Inclusion in the inertial analysis of vibration in the orientation of the pyridine ring seems justified and desirable. The planar moment analysis shows that the effect is present and appreciable, making these dimers an attractive example for the analysis. An earlier determinable case is the T-shaped Ar_2–HCl trimer,[16] where the ^{35}Cl/^{37}Cl isotope effect enabled a planar moment analysis that gave the amplitude of bending oscillations of the Ar_2 to be 7.3°. In that case, the vibrations have a significant effect (~1%) upon the interatomic distances determined. Here, it has only a small

(21) Campbell, E. J.; Buxton, L. W.; Legon, A. C. *J. Chem. Phys.* **1983**, *78*, 3483.
(22) Husson, X.; Grandin, J.-P.; Kucal, H. *J. Phys.* **1979**, *B12*, 3883.
(23) Dykstra, C. E. *J. Comput. Chem.* **1988**, *9*, 476.
(24) Applequist, J. *J. Chem. Phys.* **1984**, *85*, 279.
(25) Wang, J. H. S.; Flygare, W. H. *J. Chem. Phys.* **1970**, *52*, 5636.
(26) Dykstra, C. E., personal communication.
(27) Bauer, G. E. W.; Huiszoon, C. *Mol. Phys.* **1982**, *47*, 565.
(28) Gamba, Z.; Bonadeo, H. *J. Chem. Phys.* **1981**, *75*, 5069.
(29) Price, S. L.; Stone, A. J. *Chem. Phys. Lett.* **1983**, *98*, 419.
(30) Details of the calculation are given in the following: Ruoff, R. S. Ph.D. Thesis, University of Illinois, Urbana, 1988.

effect on R, decreasing it by about 0.004 Å in Ar–Pyr. It has a larger effect on the location of the Ar/Kr, the inclusion changing the rotation of R toward the nitrogen (γ) from −5.5° to −3.5° for Ar–Pyr. Also, when the tilt is not included, R and γ are overdetermined, and the results depend on which pair of rotational constants is employed for the determination.

Tilt was not included in the original analysis reported for the Ar–furan dimer.[7] Therefore, to make a more detailed comparison of Ar–furan with the Ar/Kr–Pyr dimers, we have analyzed its rotational constants in the same manner. The inclusion of the vibration reduces R from 3.543 to 3.541 Å and changes γ from −10.97 to −5.46°. The results are given in Table X for all of the dimers. The rotational constants used for Ar–furan are those obtained from fitting it as a prolate near symmetric top.[7]

In all three dimers with pyridine the rare-gas atom is displaced toward the heteroatom of the aromatic ring, indicating its attractive role or smaller size. The rare-gas atom to N distance in the dimers is 3.725 Å for Ar and 3.824 Å for Kr. The 0.099-Å difference is in good agreement with the difference in van der Waals radii for the two noble gases as determined from other dimers. For instance, in the HF complexes with Kr[18] and Ar,[15] the Kr to F distance is 0.1022 Å greater than the Ar to F distance. If one uses the Ar/Kr to pyridine cm distances instead, the difference is in even better agreement, 0.1027 Å.

The case of Ar–furan is somewhat different because of its pentagonal shape. It has an Ar to O distance of 3.598 Å, or 0.127 Å less than the Ar–N distance in Ar–Pyr. The difference probably reflects the smaller atomic radius and different bond hybridization of the oxygen. The furan also differs in its vibrations. The amplitude (α = 12°) is nearly double that of Ar/Kr–Pyr (α = 7°).

The force constant found in Ar–Pyr, k_s = 0.0270 mdyn/Å, is close to that reported for Ar–furan (0.0269 mdyn/Å). Also, the well depth from the simple dimer potential is essentially the same, 232 and 236 cm^{-1} for the Ar–Pyr and Ar–furan dimers, respectively. This is perhaps a little surprising since the dipole moment of pyridine is 2.18 D while for furan it is only 0.66 D. Clearly, other factors are important in determining the strength of the attraction. The k_s for ^{84}Kr–Pyr is 0.0351 mdyn/Å, or some 30% stiffer than in Ar–Pyr, and the well depth, ϵ = 322 cm^{-1}, is correspondingly larger. The larger k_s and ϵ for the krypton dimer probably reflect the greater polarizability of Kr. A similar difference is found for Kr–HF[18] versus Ar–HF.[15]

Larger clusters, Ar_mPyr_n, should exist just as for Ar_m–HF, where rotational spectra of clusters with m = 2, 3, 4 have been observed.[31-33] In fact, Levy et al. reported that a second argon, or helium, binds to the opposite side of the *s*-tetrazine ring in making the trimer Ar_2– or ArHe–tetrazine.[5] We made a search for the *b* dipole $0_{00} \rightarrow 1_{11}$ transition of an Ar_2–Pyr trimer assuming a C_{2v} structure with the second argon located like the first but on the opposite side. The value of $A + C$ predicted for this structure is 3420 MHz, but a search of ±50 MHz was unsuccessful. The transition's signal strength should have been good enough to observe, so if a second argon does go on it may not be located symmetrically with respect to the first. Another dimer of interest is Ar–benzene. An accurate determination of its structure and of the weak, induced dipole moment would be of considerable significance. We have also searched unsuccessfully for it.

Acknowledgment. This research was supported by the National Science Foundation under Grant CHE 85-20519. Acknowledgment is made to the donors of the Petroleum Research Fund, administered by the American Chemical Society, for partial support of this research. We thank Cliff Dykstra for several stimulating suggestions and discussions and particularly for help with the calculations of the ^{83}Kr EFG, with which Joe Augspurger also helped.

Registry No. Ar, 7440-37-1; ^{84}Kr, 14993-91-0; ^{83}Kr, 13965-98-5; ^{82}Kr, 14191-81-2; ^{86}Kr, 14191-82-3; Pyr, 110-86-1; [4-D]Pyr, 10259-15-1; [^{15}N]Pyr, 34322-45-7; Kr, 7439-90-9.

(31) Gutowsky, H. S.; Klots, T. D.; Chuang, C.; Keen, J. D.; Schmuttenmaer, C. A.; Emilsson, T. *J. Am. Chem. Soc.* **1987**, *109*, 5633; **1985**, *107*, 7174.
(32) Gutowsky, H. S.; Klots, T. D.; Chuang, C.; Schmuttenmaer, C. A.; Emilsson, T. *J. Chem. Phys.* **1987**, *86*, 569.
(33) Gutowsky, H. S.; Chuang, C.; Klots, T. D.; Emilsson, T.; Ruoff, R. S.; Krause, K. *J. Chem. Phys.* **1988**, *88*, 2919.

Thermochromic Shifts in Supercritical Fluids

Clement R. Yonker* and Richard D. Smith

Chemical Methods and Separations Group, Chemical Sciences Department, Pacific Northwest Laboratory,† Richland, Washington 99352 *(Received: May 3, 1988)*

Thermochromic shifts of organic solute molecules in supercritical CO_2 under conditions of both constant pressure and density are compared to previous studies of solvatochromic shifts at isothermal conditions. Similar solvatochromic and thermochromic shifts are seen as a function of density for supercritical CO_2. At constant density a small thermochromic shift (~400 cm^{-1}) for supercritical CO_2 was seen for both 2-nitroanisole and 4-ethylnitrobenzene. The excited-state dipole moments for 2-nitroanisole, as calculated from the thermochromic and solvatochromic data, were in agreement.

Introduction

Recent solvatochromic studies of supercritical fluids have provided new insights into their solvent properties, actually building a bridge between the study of the gas and liquid phases. Thermochromic shifts have been studied for the absorption spectra of select solutes in polar and nonpolar liquid solvents over a limited range of temperatures.[1] Solvatochromic shifts in supercritical fluids have been reported by various workers,[2-7] but thermochromic shifts have not been studied in detail. In thermochromic studies either pressure or density can be held constant while temperature is varied. In previous solvatochromic studies on fluids, temperature

* Address correspondence to this author.
† Operated by Battelle Memorial Institute.

(1) Suppan, P.; Tsiamis, C. *J. Chem. Soc., Faraday Trans. 2* **1981**, *13*, 1553.
(2) Sigman, M. E.; Lindley, S. M.; Leffler, J. E. *J. Am. Chem. Soc.* **1985**, *107*, 1471.
(3) Hyatt, J. A. *J. Org. Chem.* **1984**, *49*, 5097.
(4) Yonker, C. R.; Frye, S. L.; Kalkwarf, D. R.; Smith, R. D. *J. Phys. Chem.* **1986**, *90*, 3022.
(5) Frye, S. L.; Yonker, C. R.; Kalkwarf, D. R.; Smith, R. D. In *Supercritical Fluids Chemical and Engineering Principles and Applications*; Squires, T. G., Paulaitis, M. E., Eds.; ACS Symposium Series No. 329; American Chemical Society: Washington, DC, 1987; Chapter 3.

0022-3654/89/2093-1261$01.50/0